GROWTH AND CHARACTERIZATION OF TUNABLE SOLID STATE LASERS IN THE NEAR INFRARED SPECTRAL REGION

FINAL REPORT ON NASA GRANT NAG 1-694

October 30, 1990

Principal Investigators

Richard C. Powell
Joel J. Martin

Department of Physics
Oklahoma State University
Stillwater, Oklahoma 74078

INTRODUCTION

This research resulted in the publication of two major papers, that are reprinted in the following sections. The major results include the development of improved crystal growth techniques for rare earth-doped $LiYF_4$ crystals and the determination of laser-pumped laser characteristics of Tm:Ho:$Y_3Al_5O_{12}$ crystals. The students and postdoctoral research associates that participated in this work include D.W. Hart, M.G. Jani, and Roger J. Reeves.

THE GROWTH OF RARE-EARTH DOPED LITHIUM YTTRIUM FLUORIDE CRYSTALS

INTRODUCTION. The scheelite structure compound $LiYF_4$, YLF, is an excellent host for trivalent rare-earth ions. Both Bridgman and crystal pulling methods can be used to grow single crystals.[1,2,3] Both growth techniques are made more difficult because YLF melts incongruently as shown in phase diagram in Figure 1. At 819^0 C it transforms first to YF_3 and liquid. This result means that crystals must be grown from melts containing a few percent excess LiF. We are having good success using both vertical Bridgman and pulling techniques for the growth of YLF.

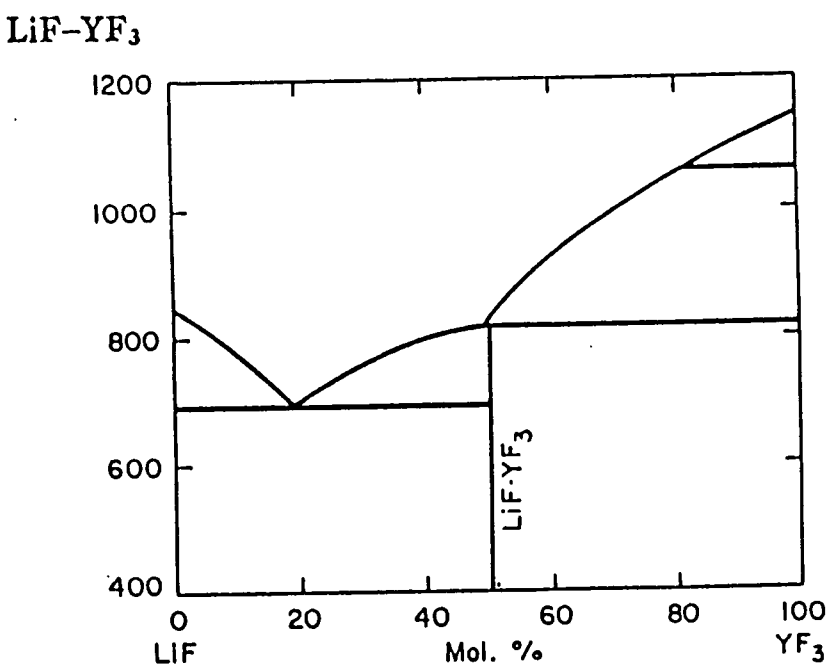

Figure 1. The phase diagram for the $LiF-YF_3$ system is shown.

RESULTS AND DISCUSSION. Commercially available rare-earth fluorides contain oxide, hydroxide and carbonate impurities that inhibit the growth of good quality crystals. These impurities can be removed (or converted) by treating the materials in HF at high temperatures. Figure 2 shows the system that we use to purify our starting materials prior to crystal growth.

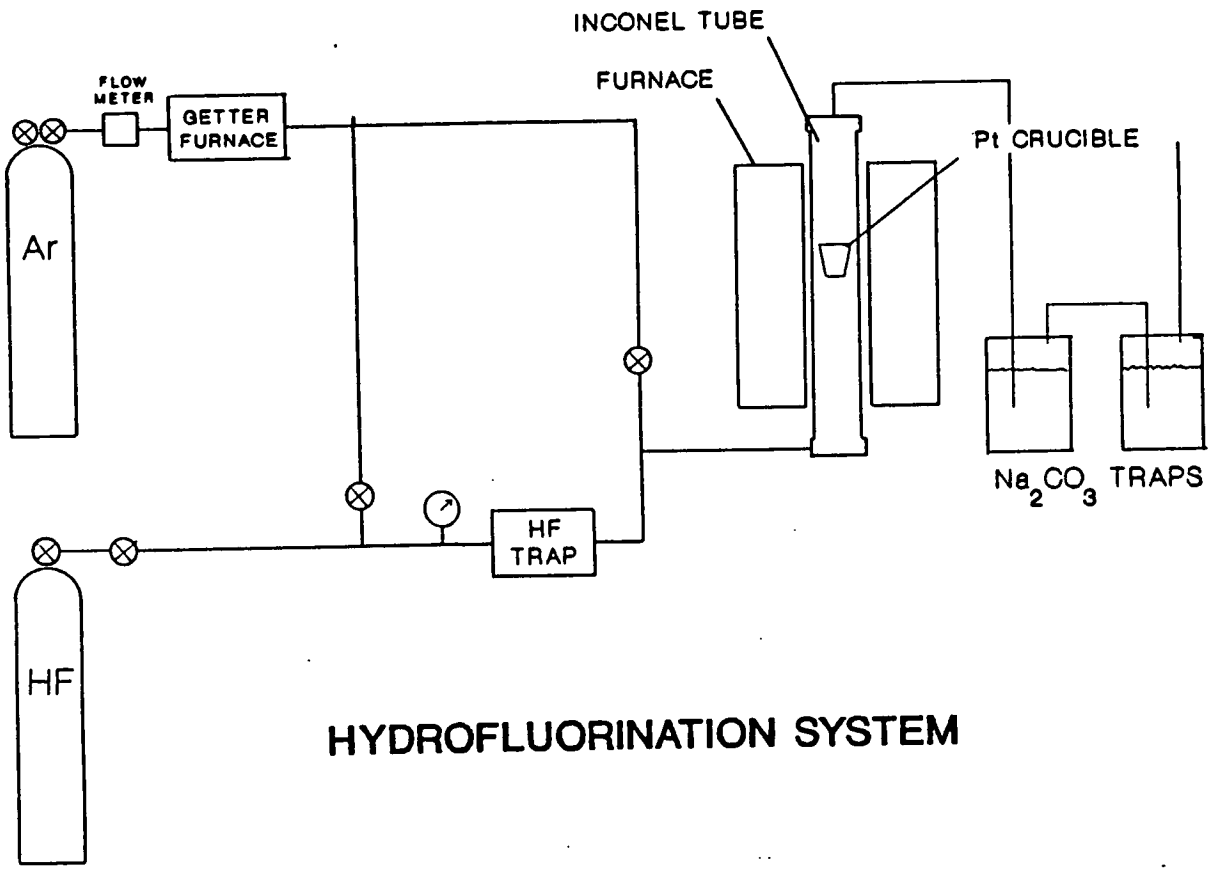

Figure 2. The system used for purifying fluoride starting materials in HF is shown.

An appropriate mixture of LiF, YF_3, and ReF_3 is placed in the platinum crucible which is then supported on an nickel rod in the furnace. A flow of gettered argon is started to purge air from the system and the furnace temperature is ramped up to 950°C

overnight. A small HF flow is started when 850°C is reached. The system is held for three hours at 950°C and then programmed down to room temperature. HF flow is maintained until the furnace has cooled below 800°C. Argon flow is continued until the furnace has cooled to room temperature and the residual HF has been purged from the system. The HF treatment produces a polycrystalline lump that is then transferred to the crystal growth furnace. It should be possible to combine the HF purification process with Bridgman growth.

During the past year we have developed a new vertical Bridgman growth system that gives a nearly 100% success rate for rare-earth doped YLF crystals. The system consists of an Applied Test System Furnace that uses Kanthal 33 heating elements with an "in-house constructed" growth chamber and crucible lower mechanism. Figure 3 shows a block diagram of the system. The vitreous carbon crucible is mounted with a carbon holder onto a nickel heat-leak rod. The heat-leak rod and a ceramic tube enclosing the crucible are supported on a moveable platform located below the furnace. At the start of a growth run the tube is evacuated to a good diffusion pump vacuum and the temperature raised to 300°C to outgas the system. The crucible is initially located near the center of the furnace. After reaching 300°C the system is backfilled with gettered argon and the temperature increased to 950°C. The melt (mp approximately 820°C is held overnight at this temperature. Then the crucible is lowered at a rate of 1.5 mm/hr through the bottom portion of the furnace. Figure 4 shows the temperature profile of the furnace.

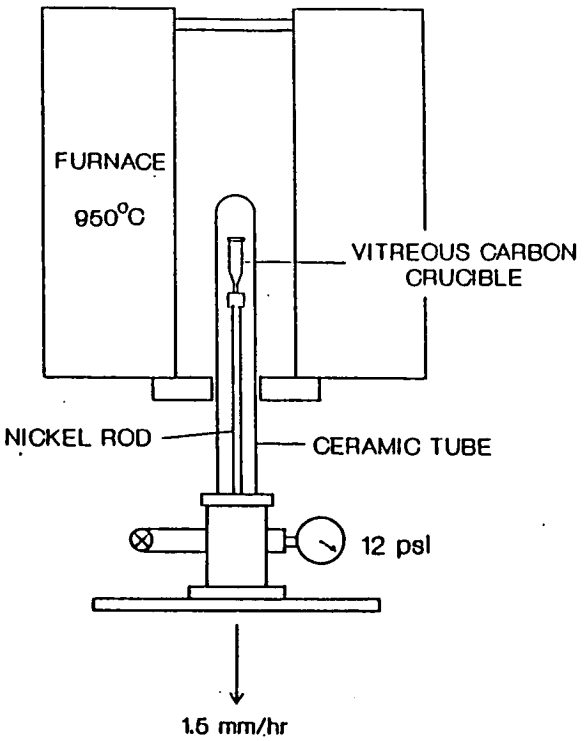

Figure 3. The new vertical Bridgman fluoride crystal growth system is shown. This system gives 100% yield.

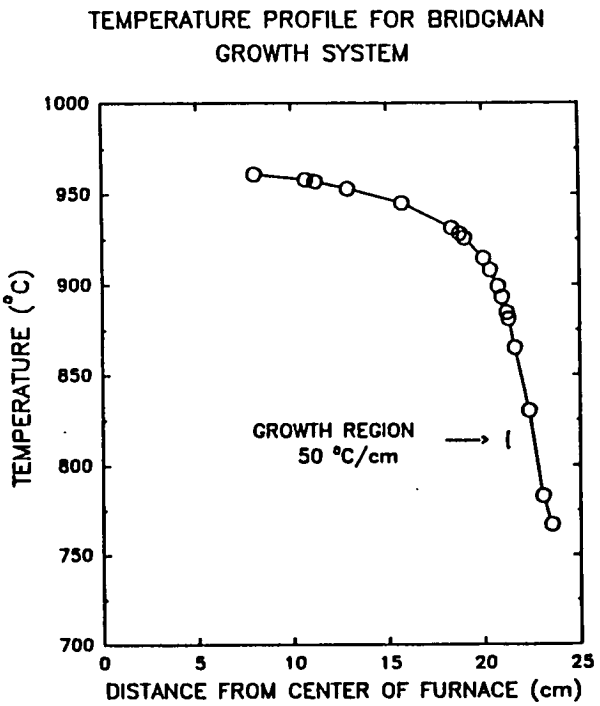

Figure 4. The temperature profile for the Bridgman system is shown.

After the crucible has cooled below 750°C the furnace is programmed back to room temperature over a 24 hour period. We feel that holding the melt at the high temperature ensures that it is well mixed. The 5°C/mm temperature gradient in this system is approximately twice that of our other systems. This larger gradient is the parameter responsible for the near 100% yield of this system. The resulting crystals are clear with a small amount of "slag" pushed to the top of the boule as shown in the photograph in Fig. 5. The slag is probably the excess LiF.

Figure 5. The photograph shows Bridgman and Czochralski YLF crystals.

At the present time we are not seeding the Bridgman growth runs. The unoriented crystals are consistently coming out with the c-axis tilted at about 30° to the long axis of the boule. The orientation of the Bridgman crystals is easily found using polarized light. We have grown a number of YLF crystals doubly doped

with Tm and Ho as well as other rare earths. The YLF:6%Tm0.2%Ho laser results discussed above and presented at the ACCG conference[4] were obtained on a Bridgman crystal.

Because of incongruent melting of YLF Cz growth is closer to top-seeded solution growth and must be done slowly. By adding additional heat shields and by developing a computer control system to slowly change the growth parameter we have solved most of our problems with the Cz growth of YLF. Figure 6 shows our crystal pulling system.

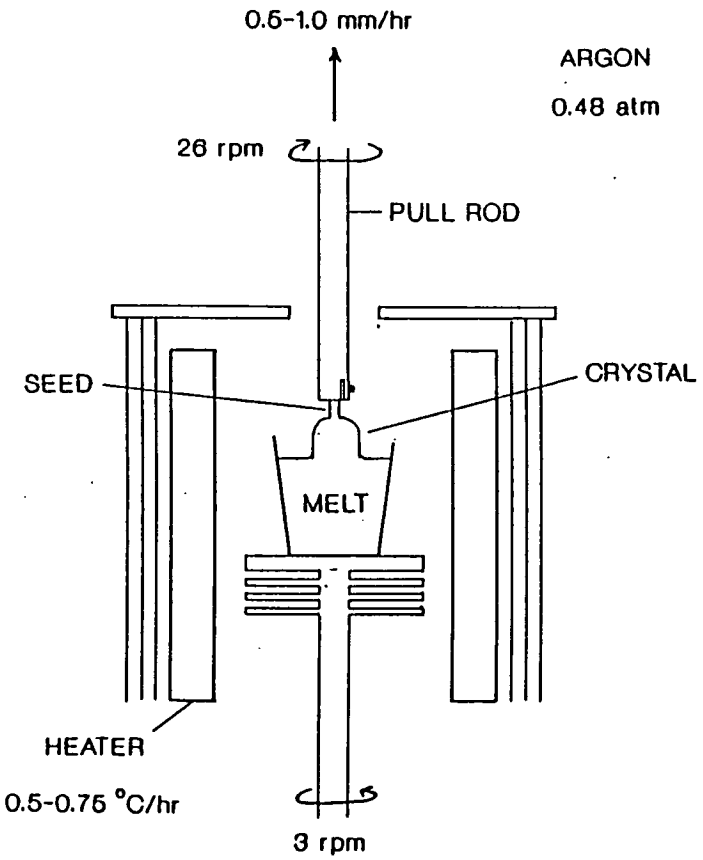

Figure 6. The crystal pulling system for fluorides is shown.

After the seed is dipped into the melt the temperature is lowered at a rate of 0.5 to 0.75°C/hr to "grow" the crystal out to the desired diameter. Once the crystal has reached the desired diameter the temperature is held nearly constant during the remainder of the growth run. A lift rates of 0.75 to 1 mm/hr have proved suitable for our system. A seed rotation rate of 26 rpm is used. We also counter rotate the crucible at 3 rpm to compensate for inhomogenities in the temperature distribution of the heater. The photograph in Figure 5 shows two of our Cz crystal boules.

CONCLUSIONS. Rare earth doped YLF crystals have been grown by both the Bridgman and Czochralski methods. Since it is much less labor intensive the Bridgman method is preferable for research samples.

REFERENCES.

1. W. A. Shand, J. Crystal Growth, 5, 143, (1969).

2. B. Cockyane, J. G. Plant, and R. A. Clay, J. Crystal Growth, 54, 407, (1981).

3. R. Uhrin, R. F. Belt, and V. Rosati, J. Crystal Growth, 38, 38 (1977).

4. D. W. Hart, C. A. Hunt, J. J. Martin, Mahendra Jani, and R. C. Powell, Eight American Conference on Crystal Growth, July 1990.

ALEXANDRITE LASER EXCITATION OF A $Tm:Ho:Y_3Al_5O_{12}$ LASER

I. INTRODUCTION

The development of room-temperature solid state lasers in the 2.0 - 3.0 μm wavelength range has received considerable attention because of potential applications in laser radar, optical communications and medicine.[1-4] Laser emission near 2.0 μm has been obtained using the $^5I_7 \dashrightarrow {}^5I_8$ transition of the Ho^{3+} ion as well as the $^3F_4 \dashrightarrow {}^3H_6$ transition of the Tm^{3+} ion in several hosts.[5-10] However, the complete details of the pumping dynamics and the optimum characteristics of laser operation have not yet been determined for these ions.

Several methods have been suggested for improving the pumping efficiency of laser crystals. Sensitization through ion-ion energy transfer is of particular interest. Room temperature, flash-lamp-pumped operation of $Ho:Y_3Al_5O_{12}$(YAG) and $Ho:LiYF_4$(YLF) lasers sensitized with Er^{3+} and Tm^{3+} ions showed that energy transfer allowed more efficient absorption of the pump light and hence higher pumping density.[6-7] For the codoped $Tm^{3+}:Ho^{3+}:Y_3Al_5O_{12}$(YAG) crystal, the $^3H_4$ manifold of Tm^{3+} can be pumped by a tunable alexandrite laser. Subsequently a Tm^{3+} ion in this level decays nonradiatively by cross-relaxation yielding two Tm^{3+} ions in the $^3F_4$ level. The excited Tm^{3+} ions then transfer their excitation energy to the $^5I_7$ level of Ho^{3+} ions which is the upper level for laser emission near 2.0 μ m. Room temperature operation of a Ho^{3+} laser pumped with an alexandrite laser was first reported by Kintz, et al.[8] In their study, a $Tm^{3+}:Ho^{3+}$:YAG laser crystal with its ends coated to create a monolithic optical resonator was optically pumped at a wavelength of 785 nm with a 200 μs pulse from an alexandrite laser. The

maximum slope efficiency obtained was 65.8%.

In this paper we report laser emission from a Tm^{3+}:Ho^{3+}:YAG crystal excited with multiple pump wavelengths. The threshold and slope efficiency as well as the spectral, spatial and temporal profiles of the laser emission were investigated as the pump laser energy, wavelength and repetition rates were varied. The laser emission from the Tm:Ho:YAG crystal was comprised of several wavelengths that may allow some tuning of emission. A comparison between a monolithic crystal resonator and an external cavity configuration was also performed.

II. EXPERIMENTAL PROCEDURE

The laser crystal used in this study was grown by the standard Czochralski technique. The doping levels are 8.3 x $10^{20}cm^{-3}$ of Tm^{3+} ions and 6.9 x $10^{19}cm^{-3}$ of Ho^{3+} ions. The room temperature absorption spectrum, shown in Fig. 1 , was measured using a Beckman 4240 spectrophotometer. The absorption bands[11] centered at 780 nm and 785 nm are attractive for diode laser pumping[2] and are in an appropriate region for excitation by an alexandrite laser. We have also studied a YAG crystal containing 7.9 x 10^{20} cm^{-3} of Tm^{3+} ions and 8.3 x 10^{18} cm^{-3} of Ho^{3+} ions which had its end faces coated to create a monolithic optical resonator.

A multi-mode alexandrite laser with a tuning range of 720 nm to 820 nm was used as a monochromatic pump source. The pump laser could be operated at repetition rates from 5-20 Hz and its output consisted of a series of 300 ns pulses in a 60 μs envelope. A longitudinal pumping configuration was used with the cavity

consisting of a 1-m radius of curvature high reflector and a flat output coupler placed 10 cm apart. The high reflector was coated to transmit light between 700 and 800 nm and reflect light between 1.8 and 2.2 μm. The flat output coupler had 2% transmission between 1.8 and 2.2 μm. The pump beam diameter was measured using a burn paper and found to be approximately 2 mm. The laser crystal was cut and polished to a 2.3 mm thickness and antireflection coated for light in the 1.8 - 2.2 μm region. For this crystal thickness approximately 63% of incident pump light is absorbed at 785 nm, 62% at 780 nm, and 34% at 765 nm, which are the pump wavelengths used in this study. The laser crystal used for the monolithic optical resonator was 2 mm thick with one end flat acting as a high reflector between 1.8-2.2 μm and highly transmitting at 785 nm. The other end was a concave reflector with a 10 mm radius of curvature and 99.5% reflecting between 1.8-2.2 μm. Residual pump light was blocked by a germanium filter and the laser output was monitored either with an energy meter or passed through a monochromator to a detection system.

III. RESULTS AND DISCUSSION

An excitation spectrum of laser emission at 2.1 μm was recorded by continuously scanning the alexandrite laser wavelength while an InSb detector monitored the laser emission from the cavity. The results obtained are shown in Fig. 2. The excitation spectrum contains lines that correspond to absorption transitions to various Stark levels within the $^3H_4$ manifold of the Tm^{3+} ion. Of interest was the fact that the Tm:Ho:YAG crystal

lased at several alexandrite pump wavelengths. Three of the pump wavelengths were chosen to further characterize the lasing properties.

The laser slope efficiencies and threshold energies were measured as a function of the wavelength and repetition rates of the pump laser. Results of these studies are shown in Fig. 3 (a), (b), and (c) for pump wavelengths of 765 nm, 780 nm, and 785 nm, respectively. The measured values of slope efficiencies and threshold energies are listed in Table 1. The maximum slope efficiency of 15.6% was obtained for a pumping wavelength of 780 nm and 10 Hz repetition rate. In Fig. 3 (b) and (c) four data points at the higher absorbed energies were not included for calculation of slope efficiencies. The roll off in these data points is due to thermal effects at high pumping energies. Additional losses arising from our use of an external cavity probably account for the lower efficiencies measured here compared with results from a monolithic cavity.[8] Also, no external lens was used to maximize the coupling of pump light into the cavity mode volume because of potential surface damage to the crystal. The slope efficiency for a pump wavelength of 765 nm was a factor of two lower than the value at 780 nm. The purpose of the work described here was not to maximize the slope efficiency but rather to characterize the changes in laser characteristics for different pumping conditions. The temporal properties of the same monolithic optical resonator crystal used by Kintz et. al.[8] were measured for comparison with our sample but the slope efficiency was not remeasured.

In previous studies green fluorescence between 528 nm and

561 nm was observed from a Tm:Ho:YAG crystal when excited with 780 nm light.[12-14] Tyminski, et al.[12] assigned the green luminescence to cooperative energy transfer processess populating the $^5F_4$, $^5S_2$ level of the Ho^{3+} ion. We have measured the intensity of this fluorescence for the three alexandrite laser wavelengths used and the results are shown in Fig. 4. Although the absorbed energy at the pump wavelength of 765 nm is less than at either 780 or 785 nm, the intensity of the green fluorescence is much higher. This observation suggests that the upconversion processes producing this green fluorescence are probably responsible for the reduced laser slope efficiency at the 765 nm excitation wavelength. An excitation spectrum for the green fluorescence was recorded and the results are shown in Fig. 5. The salient features of this spectrum are that alexandrite laser wavelengths shorter than 770 nm are much more efficient at producing the green fluorescence than longer wavelengths, and that there are many more spectral lines observed than are expected from the absorption spectrum. This last observation may indicate that excited state absorption processes involving pump photons contribute to the upconversion.

The green fluorescence observed originates from the $^5F_4$,$^5S_2$ manifolds of the Ho^{3+} ion excited by some type of upconversion process as shown in Fig. 6. A process that may populate this level is cooperative energy transfer between Tm^{3+} and Ho^{3+} ions which is known to occur at room temperature and high excitation intensities. Once the Ho^{3+} $^5I_7$ level has been populated further pumping of Tm^{3+} can deplete the population in this upper laser

level through upconversion energy transfer processes. Phonon-assisted back-transfer from Ho^{3+} to Tm^{3+} may also result in some depletion of the $^5I_7$ population.

While the above mentioned processes play a role in the efficiency of the laser, their influence will not change with pump wavelength and they are not contributing to the additional green fluorescence observed here at short pump wavelengths. The transitions from the $^5I_7$ upper laser level to the $^5F_4$,$^5S_2$ green-emitting levels of the Ho^{3+} ion, are a close match to the wavelength of the alexandrite laser and the excited state absorption of pump laser photons is possible. Tyminski, et al.[12] reported that the green luminescence excited by 5 ns pulses rises with the time constant of 12 to 30 μs. This supports the cooperative energy transfer mechanism populating the $^5F_4$,$^5S_2$ level. However, under our experimental conditions both the cooperative process and the excited state absorption of pump photons are most likely contributing to the green luminescence.

The requirement for an efficient excited state absorption process is that the absorption rate of pump photons from the excited level must be comparable to or greater than the decay rates of the level. The $^5I_7$ level of interest here is a metastable state with a lifetime of 6 ms and will likely satisfy this requirement for the high intensity alexandrite pumping. The situation will be different when the crystal is in an optical cavity and lasing. Stimulated emission will depopulate the $^5I_7$ level decreasing the amount of pump photon excited state absorption that is occurring. This is in fact observed as the amount of green fluorescence decreases when the crystal is

lasing.[15]

The spectral distribution of the laser emission was monitored using a 0.25-m SPEX monochromator (0.25 mm slits) with a grating blazed at 2.0 μm (300 grooves/mm) and an InSb detector. Simultaneous free-running laser emission was observed at 2.060, 2.065, 2.097 and 2.101 μm as shown in Fig. 7 for 780 nm pumping. The same laser emission peaks were also observed for pump wavelengths of 765 nm and 785 nm. As the absorbed pump energy increases, the laser emission peaks at 2.097 and 2.101 μm start to grow rapidly in comparison to the laser peaks at 2.060 and 2.065 μm as shown in Fig. 7. Although it is difficult to make unambiguous assignments of different emission wavelengths to transitions between specific Stark levels, the wavelengths observed here are assigned as follows. The laser transition at 2.101 μm is between the Stark level at 5250 cm^{-1} of $^5I_7$ manifold and the thirteenth level at 494 cm^{-1} in the $^5I_8$ ground state manifold. The laser emission at 2.097 μm is between the lowest Stark level at 5229 cm^{-1} and the twelfth Stark level at 460 cm^{-1} in the ground state manifold. Similarly the laser transition at 2.065 μm is between the Stark level at 5304 cm^{-1} and the level at 460 cm^{-1} and the laser emission at 2.060 μm is between the level at 5314 cm^{-1} and the level at 460 cm^{-1}. Since the stimulated emission cross-section for the 2.097 μm transition is higher than those of the other transitions, the gain for this line increases rapidly once population inversion is attained. Thus this line will oscillate if the round-trip losses are sufficiently high to overcome the gain at other wavelengths. The

emission lines at 2.060 and 2.065 μm become more prominent at higher pump energies as the upper Stark components of $^5I_7$ level are populated due to thermal effects according to a Boltzmann distribution leading to higher energy laser emission from these levels. Thermal heating of the sample is due to phonons generated from raditionless relaxation processes associated with the optical pumping dynamics.

Figure 8 shows the emission intensities obtained for the different laser emission peaks as a function of absorbed pump energies. The emission peak at 2.097 μm has the highest slope efficiency. The differences in the efficiencies can be associated with thermal effects affecting the population of the upper laser levels in the $^5I_7$ manifold of Ho^{3+} ions and the emission cross sections associated with these Stark levels.

Temporal properties of the laser emission and pump pulses were recorded using an InSb detector and a Tektronix digital oscilloscope. Figure 9 shows the time evolution of laser emission following the alexandrite excitation pulse at 780 nm for several different pump energies. Similar results were observed for pumping wavelengths of 765 nm and 785 nm. The spiking behavior observed in Fig. 9 is due to relaxation oscillations normally observed in solid state lasers. There is a delay time between the alexandrite pump pulse and the beginning of lasing emission. The interesting results seen in this figure are that the delay time and the shape of the lasing pulse are sensitive to absorbed pump energy. The delay time decreases and the pulse width increases for the laser emission with an increase in pump energy. This implies that the spectral features of the gain are inhomogeneous.

The temporal profile of laser emission from a monolithic crystal resonator obtained from the Naval Research Laboratory is shown in Fig. 10. The emission observed at long delay times is similar to that seen in an open optical cavity as described in the previous paragraph. However, for the monolithic cavity there is an additional laser emission spike with a delay time of approximately 10 μs. This additional spike is probably due to laser emission from Tm^{3+} ions at 2.0 μm. It is not observed in the open cavity configuration due to higher losses and greater absorption of the 2.0 μm wavelength by water vapor in the surrounding atmosphere.

The excited state dynamics in co-doped Tm:Ho:YAG crystals are dominated by the following three processes:[16] (i) radiationless relaxation from $^3H_4$ level to $^3H_5$ level in the Tm^{3+} ions; (ii) the cross-relaxation process between two Tm^{3+} ions of type $^3H_4, ^3H_6$ ---- $^3F_4, ^3F_4$; and (iii) the energy transfer from the $^3H_4$ level of Tm^{3+} ions to the $^5I_5$ level of Ho^{3+} ions. It has been reported[17] that for Tm-doped YAG, the Tm-Tm cross relaxation time is 10 μs for 4 x 10^{20} cm^{-3} Tm^{3+} ions and is rduced to 3μs for 10 x 10^{20} cm^{-3} Tm^{3+} ions. The energy transfer from Tm^{3+} to Ho^{3+} ions takes place in about[17] 5 μs. This implies that the feeding time for the $^5I_7$ level of Ho^{3+} ions should be about 10-20 μs which would be the delay time for 2.1 μm lasing emission. Our results show the shortest delay times to be 60 μs at the highest absorbed energy and for pumping wavelengths of 780 nm and 785 nm. The longer delay times observed here may be associated either with oscillation build up or other processes involving pumping

dynamics such as long range energy migration among Tm^{3+} ions prior to energy transfer to Ho^{3+} ions. Four-wave mixing experiments are in progress to try to answer this question.

IV. CONCLUSIONS

In summary, the results presented here show multiple wavelength laser emission at room temperature in Tm:Ho:YAG pumped with an alexandrite laser. The different laser emission wavelengths exhibited different slope efficiencies associated with the pumping dynamics of the system. The laser emission was found to be sensitive to the pump wavelength with the highest slope efficiency obtained for 780 nm excitation. The pump wavelength dependence was found to be due to upconversion processes associated with excited state absorption of pump photons. These processes had only a small effect on the slope efficiency for 780 and 785 nm pump wavelengths, but significantly reduced the slope efficiency for 765 nm excitation. The temporal profiles of the laser emission exhibit time delays and pulse width changes as a function of pump power. These are associated with the pumping dynamics of this material and indicate the presence of long range energy migration among Tm^{3+} ions. An increase in spectral and temporal widths was observed as a function of pump energy indicating presence of additional lasing modes. A monolithic crystal resonator showed additional laser emission that may originate from Tm^{3+} ions.

The results of this study show the complex nature of the pumping dynamics of the Tm,Ho:YAG laser system. This indicates the need for a detailed investigation of the relationships

between the laser properties and the physical processes contributing to the pumping dynamics of the system.

ACKNOWLEDGMENTS

This work was sponsored by NASA Langley Research Center under Grant number NAG-1-694. The authors benefited greatly from many helpful discussions with R.V. Hess and C.H. Bair.

REFERENCES

1. G. J. Kintz, L. Esterowitz, and R. Allen, "CW Diode-Pumped Tm^{3+},Ho^{3+}: YAG 2.1 μm Room-Temperature Laser," "Electron. Lett. 23, 616 (1987).

2. T. Y. Fan, G. Huber, R. L. Byer, and P. Mitzscherlich, Opt. " Continuous-Wave Operation at 2.1 μm of a diode-laser-pumped, Tm-sensitized Ho:$Y_3Al_5O_{12}$ laser at 300 K," Opt. Lett. 12, 678 (1987).

3. G. J. Kintz, L. Esterowitz, and R. Allen, " Cascade Laser Emission at 2.31 and 2.08 μm from Laser Diode Pumped Tm:Ho:$LiYF_4$ at Room Temperature," in Digest of Topical Meetings on Tunable Solid-state Lasers, (Optical Society Of America, Washington, D.C., 1987) paper MC2-1.

4. G. J. Quarles, A. Rosenbaum, C. L. Maquardt, and L. Esterowitz, " Efficient room-temperature operation of a flash-lamp-pumped, Cr,Tm:YAG laser at 2.01 μm," Opt. Lett. 15, 42 (1990).

5. L. F. Johnson, G. D. Boyd, and K. Nassau, " Optical Maser Characteristics of Ho^{3+} in $CaWO_4$," Proc. IRE 50, 86 (1962).

6. R. L. Remski and D. J. Smith, "Temperature Dependence of Pulsed Lase Threshold in YAG: Er^{3+}, Tm^{3+}, Ho^{3+}," IEEE J. Quantum Electron. 6, 750 (1970).

7. E. P. Chicklis, C. S. Naiman, R. C. Fulweiler, D.R. Gabbe, H. P. Jenssen, and A. Linz, " High Efficiency Room-Temperature 2.06 μm Laser Using Sensitized Ho^{3+}: YLF," Appl. Phys. Lett. 19, 119 (1971).

8. G. J. Kintz, R. Allen, and L. Esterowitz, " Two for One Photon Conversion Observed in Alexandrite Pumped Tm^{3+},Ho^{3+}:

YAG at Room Temperature," in Digest of the Conference on Lasers and Electro-optics, (Optical Society of America, Washington, D.C., 1987), postdeadline paper ThU4-1.

9. H. Hemmati, " 2.07-μm CW diode-laser-pumped Tm,Ho: $YLiF_4$ room-temperature laser," Opt. Lett. 14, 435 (1989).

10. R. C. Stoneman and L. Esterowitz, " Efficient, broadly tunable, laser-pumped Tm: YAG and Tm: YSGG cw lasers," Opt. Lett. 15 , 486 (1990).

11. J. B. Gruber, M. E. Hills, R. M. Macfarlane, C. A. Morrison, G. A. Turner, G. J. Quarles, G. J. Kintz, and L. Esterowitz, " Spectra and energy levels of Tm^{3+}: $Y_3Al_5O_{12}$," Phys. Rev. B 40, 9464 (1989).

12. J. K. Tyminski, D. M. Franich, and M. Kotka, " Gain dynamics of Tm:Ho: YAG pumped in near infrared," J. Appl. Phys. 65, 3181 (1989).

13. T. Y. Fan, G. Huber, R. L. Byer and P. Mitzscherlich, " Spectroscopy and Diode Laser-Pumped Operation of Tm:Ho: YAG,"IEEE J. Quantum Electron. 24, 924 (1988).

14. G. J. Kintz, I. D. Abella, and L. Esterowitz, " Upconversion Coefficient measurement in Tm:Ho: YAG at Room Temperature," in Proceedings of the International Conference on Lasers'87 (STS, McLean, Va.,1988),p.398

15. R. C. Stoneman and L. Esterowitz, Naval Research Laboratory, Washington, D.C. 20375-5000 (personal communication, 1990).

16. A. Brenier, R. Moncorge, and C. Pedrini, " Fluorescence Dynamics in $LiYF_4$: Tm, Ho after 800-nm Laser Excitation," in Proceedings of Tunable solid State Lasers Conference. 5 ,

(Optical Society of America, Washington, D.C., 1989), p. 232.

17. T. Becker, R. Clausen, and G. Huber, " Spectroscopic and Laser Properties of Tm-Doped YAG at 2 μm," in Proceedings of Tunable Solid State Lasers Conference. 5 ,(Optical Society of America, Washington, D.C., 1989), p. 150.

TABLE I. Thresholds and slope efficiencies for a Tm,Ho:YAG laser with different pump wavelengths at repetition rate of 10 Hz.

PUMP λ	THRESHOLD ENERGY	EFFICIENCY
765 nm	7 mJ	7.1 %
780 nm	11 mJ	15.6 %
785 nm	11 mJ	10.5 %

FIGURE CAPTIONS

Fig. 1. Room-temperature absorption spectrum of a 2.3 mm thick Tm:Ho:YAG crystal in the region of alexandrite laser excitation.

Fig. 2. Laser excitation spectrum for the 2.1 μm emission of Tm:Ho:YAG. The numbers above the curve represent absorbed pump energy.

Fig. 3. Energy threshold and slope efficiencies of Tm:Ho:YAG laser emission for different pump wavelengths. (a) 765 nm, (b) 780 nm, (c) 785 nm. The numerical results from these data are listed in Table I. The repetition rate for the pump laser was 10 Hz.

Fig. 4. Green fluorescence of Tm:Ho:YAG for different pump wavelengths. (a) 765 nm excitation, absorbed pump energy 15.4 mJ. (b) 780 nm excitation, absorbed pump energy 26.4 mJ. (c) 785 nm excitation, absorbed pump energy 28.9 mJ.

Fig. 5. Excitation spectrum for green-fluorescence at 538 nm from Tm:Ho:YAG crystal.

Fig. 6. Pumping diagram for Tm:Ho:YAG laser. Upconversion may be due to either cooperative energy transfer and/or excited state absorption of pump photons.

Fig. 7. Spectral distribution of laser emission of Tm:Ho:YAG in an external cavity as a function of absorbed pump energy.

Fig. 8. Energy thresholds and slope efficiencies of Tm:Ho:YAG for different laser emission peaks.

Fig. 9. Temporal profiles of the Tm:Ho:YAG laser emission as a

function of absorbed pump energy in an external cavity configuration. The top most curve shows alexandrite laser pump pulse and the curves below it represent the Tm:Ho:YAG laser emission.

Fig. 10. Temporal profiles of the Tm:Ho:YAG laser emission in a monolithic crystal cavity. (a) Alexandrite pump pulse and (b) Tm:Ho:YAG laser emission.

Figure 1

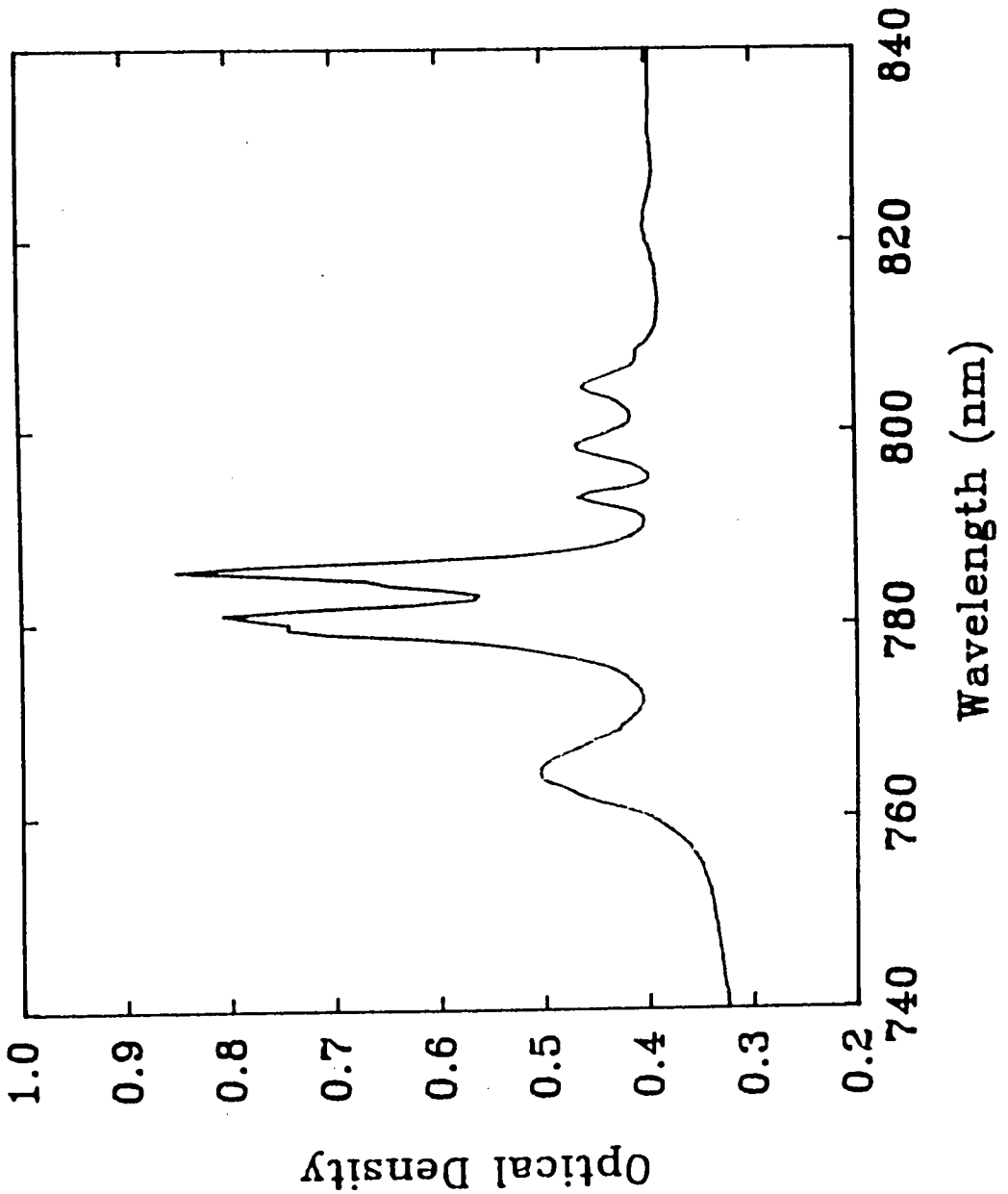
Optical Density
1.0
0.9
0.8
0.7
0.6
0.5
0.4
0.3
0.2
740
760
780
800
820
840
Wavelength (nm)

Figure 2.

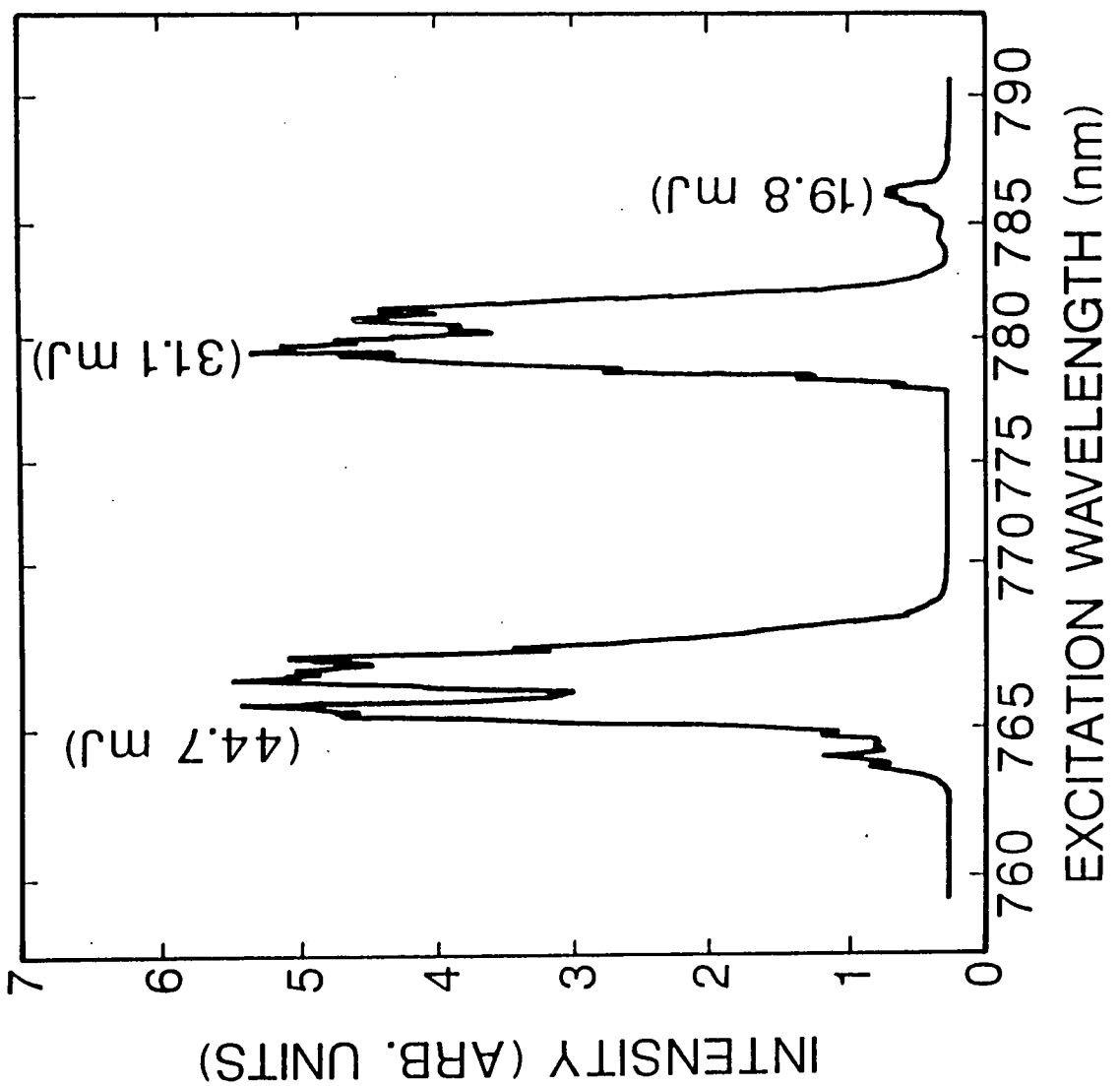
INTENSITY (ARB. UNITS)
0
1
2
3
4
5
6
7
760
765
770
775
780
785
790
EXCITATION WAVELENGTH (nm)
(44.7 mJ)
(31.1 mJ)
(19.8 mJ)

Figure 3

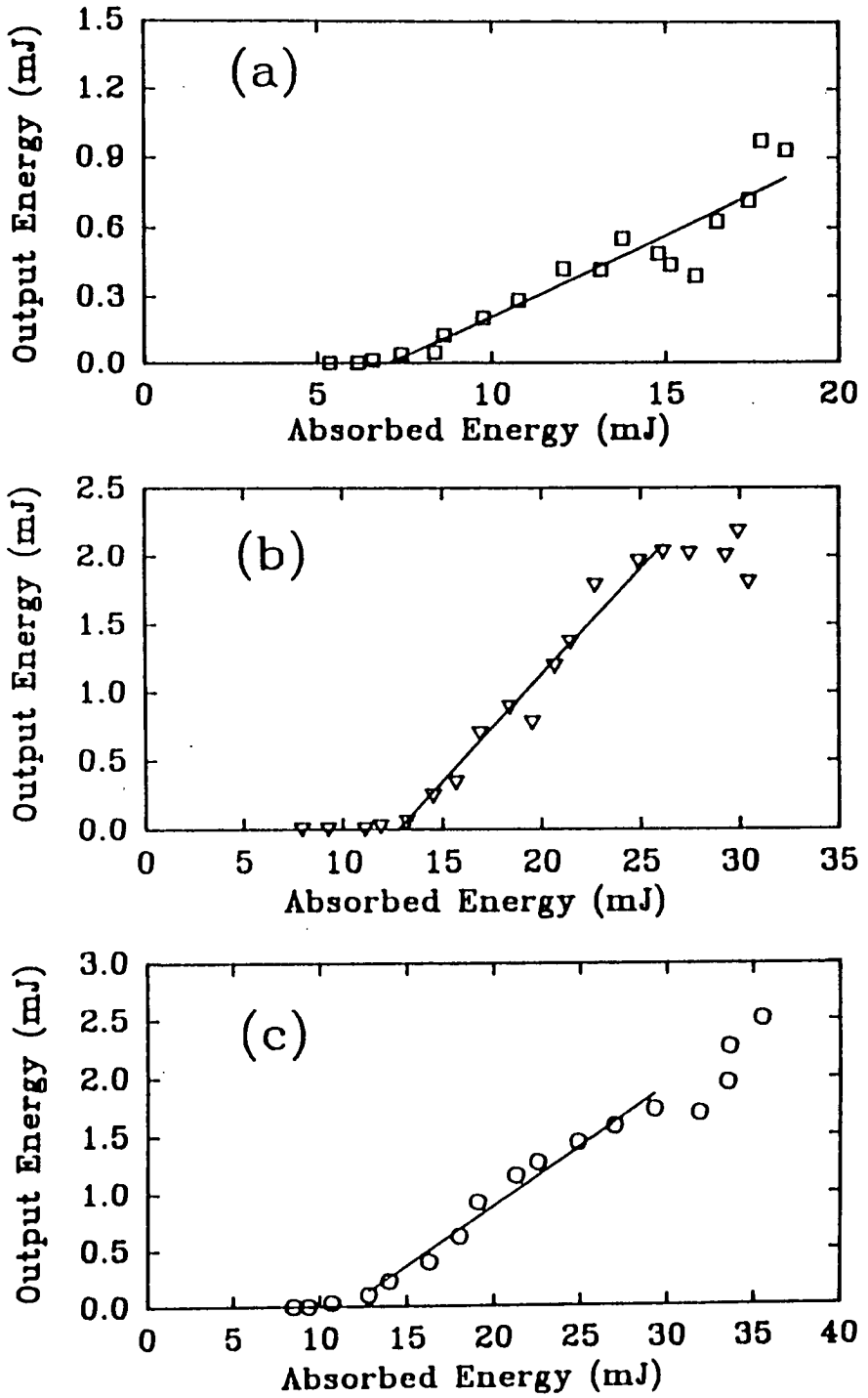
(a)
Output Energy (mJ)
Absorbed Energy (mJ)
0.0
0.3
0.6
0.9
1.2
1.5
0
5
10
15
20
(b)
Output Energy (mJ)
Absorbed Energy (mJ)
0.0
0.5
1.0
1.5
2.0
2.5
0
5
10
15
20
25
30
35
(c)
Output Energy (mJ)
Absorbed Energy (mJ)
0.0
0.5
1.0
1.5
2.0
2.5
3.0
0
5
10
15
20
25
30
35
40

Figure 4.

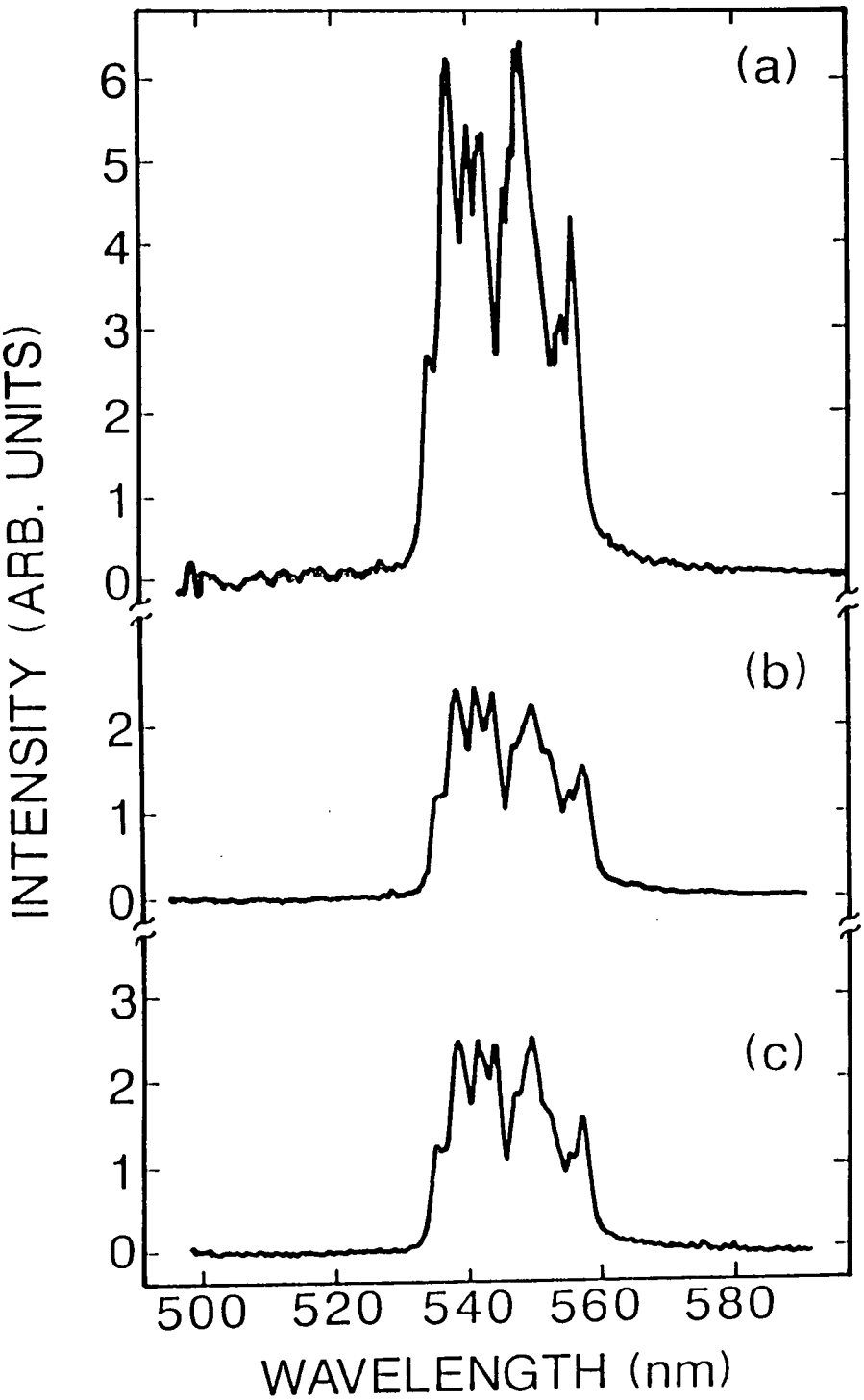
(a)
(b)
(c)
INTENSITY (ARB. UNITS)
0
1
2
3
4
5
6
500
520
540
560
580
WAVELENGTH (nm)

Figure 5.

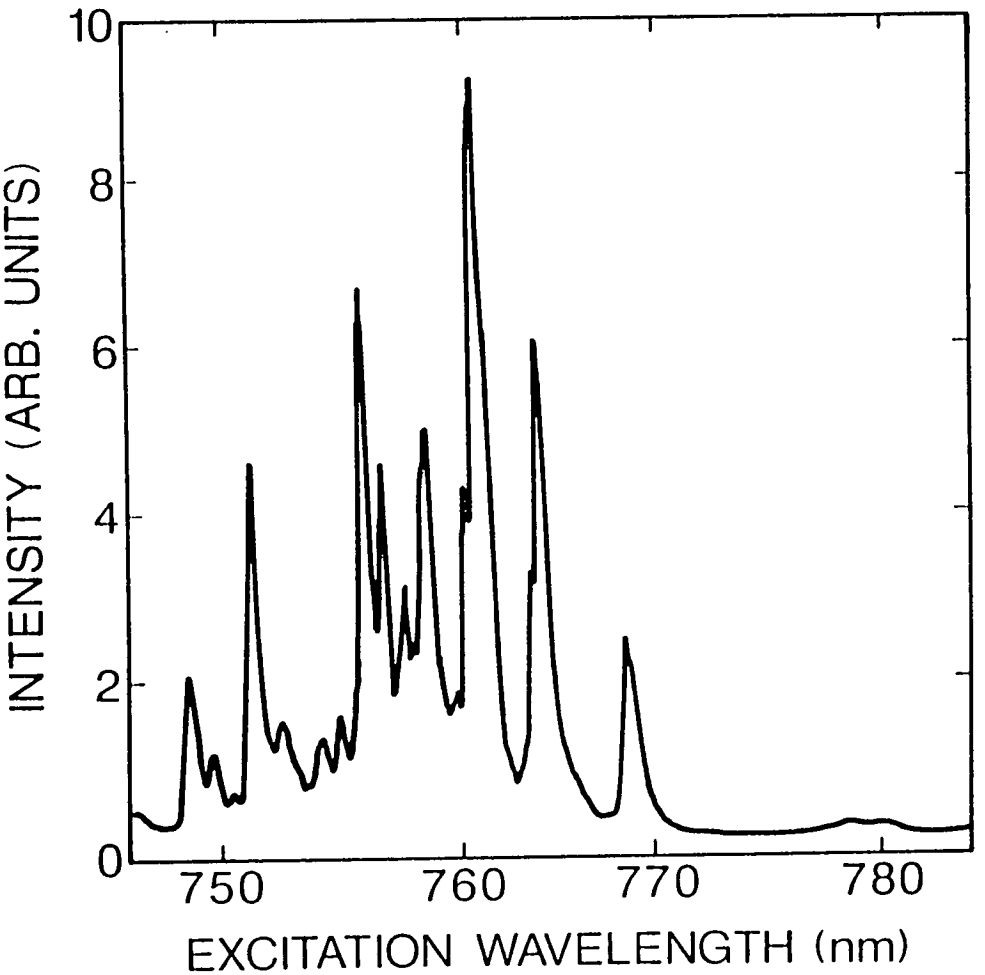
10
8
6
4
2
0
INTENSITY (ARB. UNITS)
750
760
770
780
EXCITATION WAVELENGTH (nm)

Figure 6

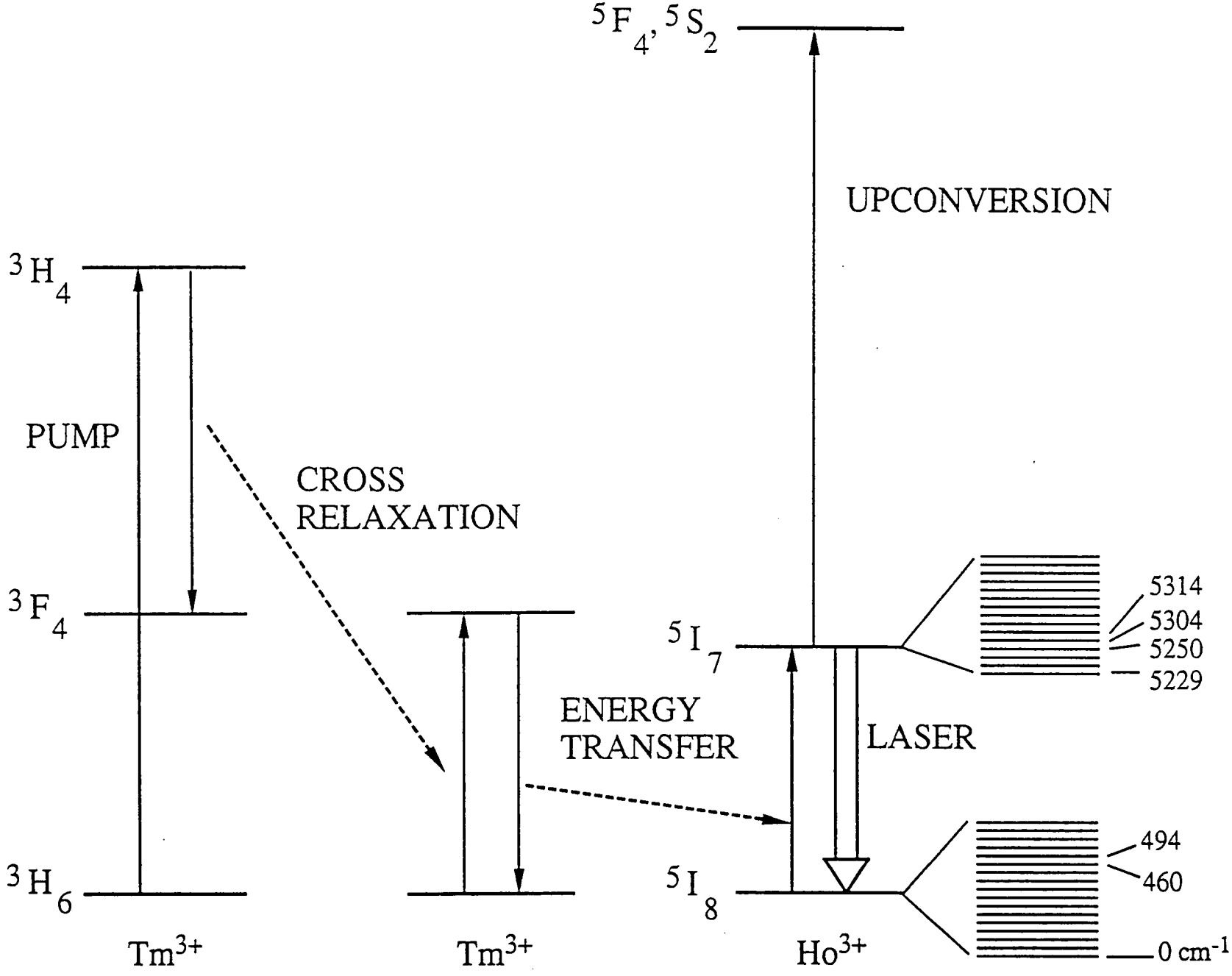
$^5F_4, ^5S_2$
UPCONVERSION
$^3H_4$
PUMP
CROSS
RELAXATION
$^3F_4$
$^5I_7$
5314
5304
5250
5229
ENERGY
TRANSFER
LASER
$^3H_6$
$^5I_8$
494
460
0 cm^{-1}
Tm^{3+}
Tm^{3+}
Ho^{3+}

Figure 7.

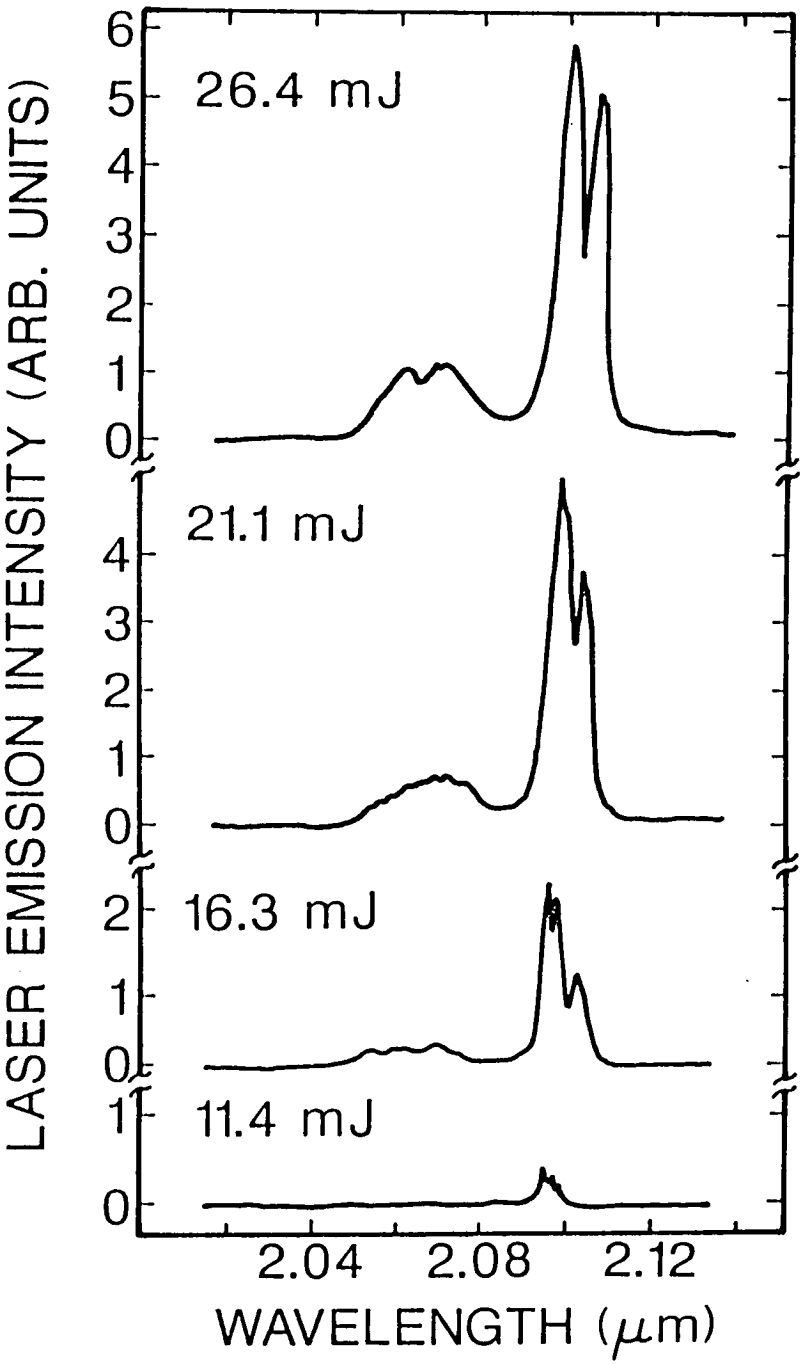
LASER EMISSION INTENSITY (ARB. UNITS)
26.4 mJ
21.1 mJ
16.3 mJ
11.4 mJ
6
5
4
3
2
1
0
4
3
2
1
0
2
1
0
1
0
2.04
2.08
2.12
WAVELENGTH (μm)

Figure 8

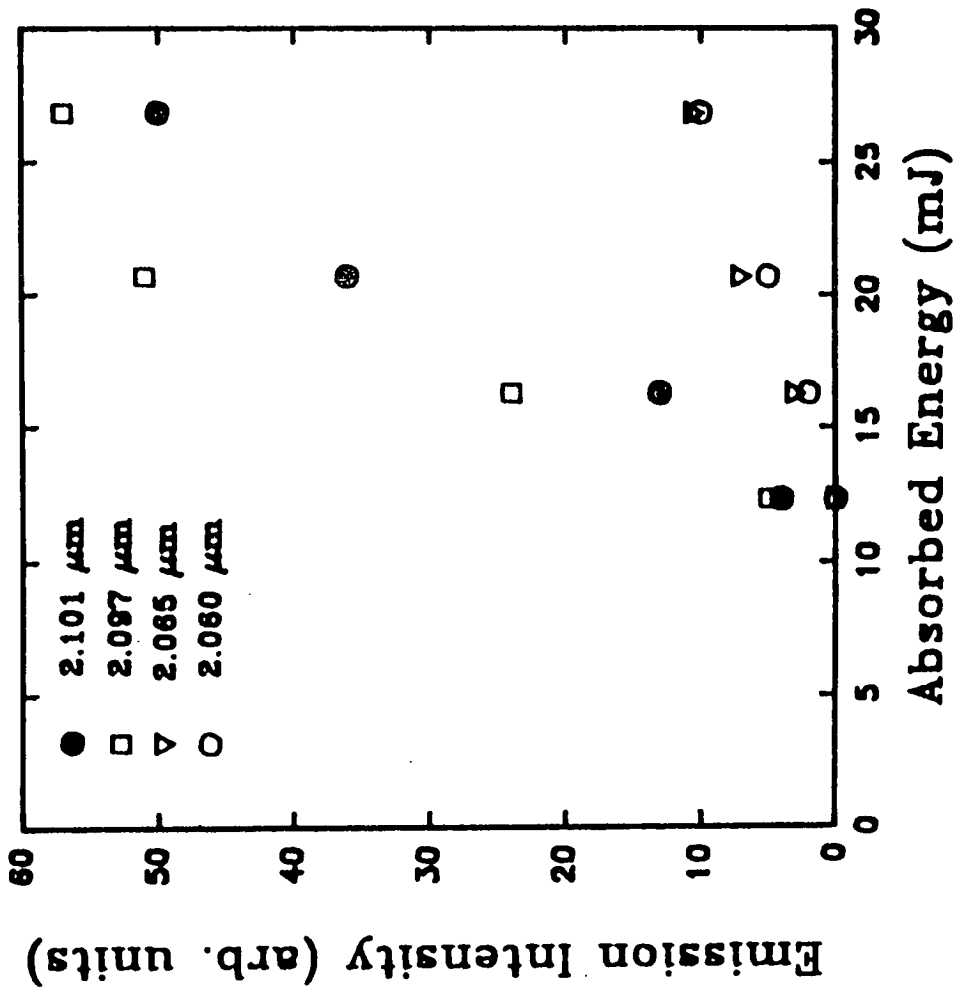
Emission Intensity (arb. units)
Absorbed Energy (mJ)
2.101 μm
2.097 μm
2.085 μm
2.060 μm
0
10
20
30
40
50
60
0
5
10
15
20
25
30

Figure 9.

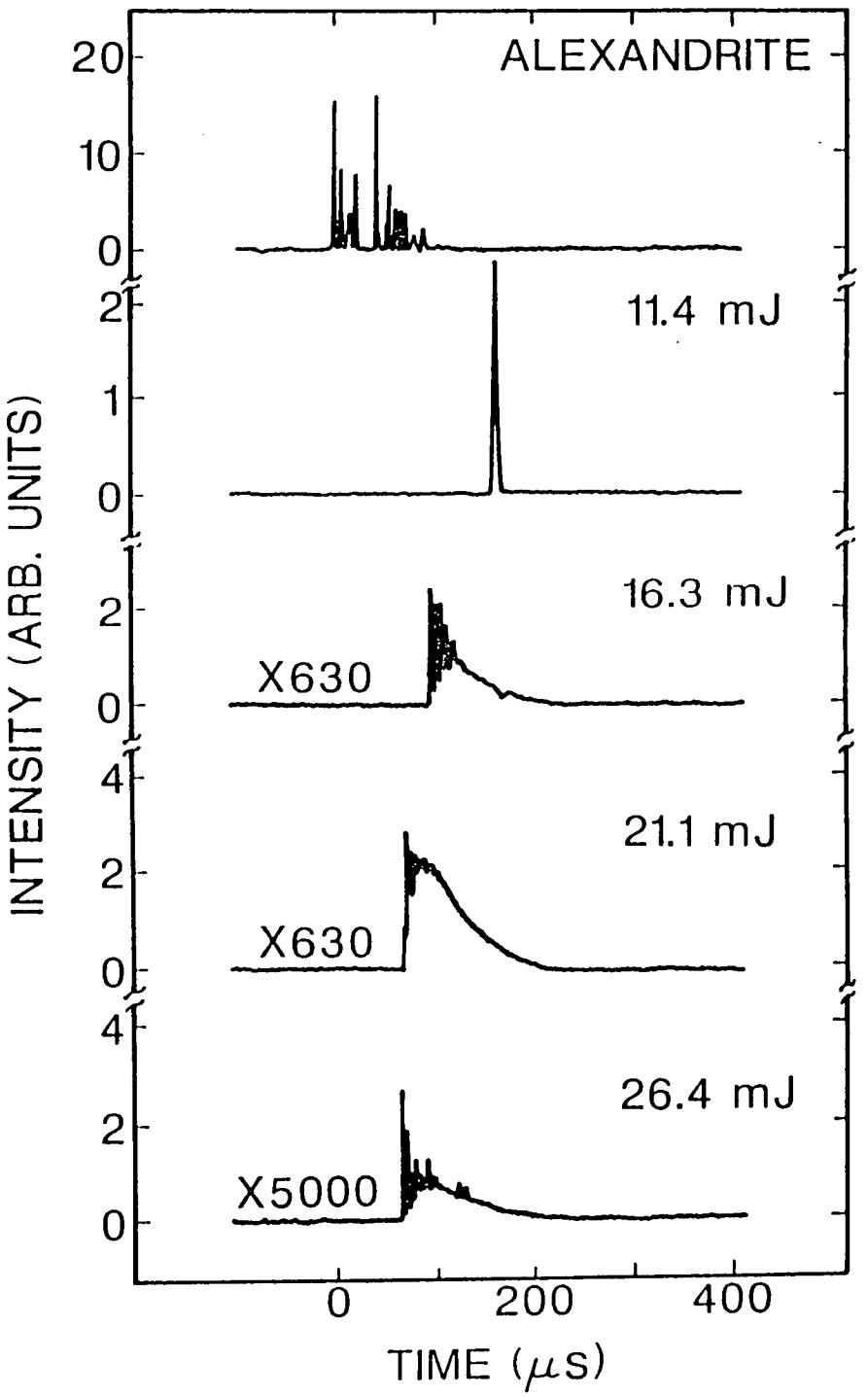
ALEXANDRITE
11.4 mJ
16.3 mJ
X630
21.1 mJ
X630
26.4 mJ
X5000
INTENSITY (ARB. UNITS)
TIME (μs)
0
200
400

Figure 10.

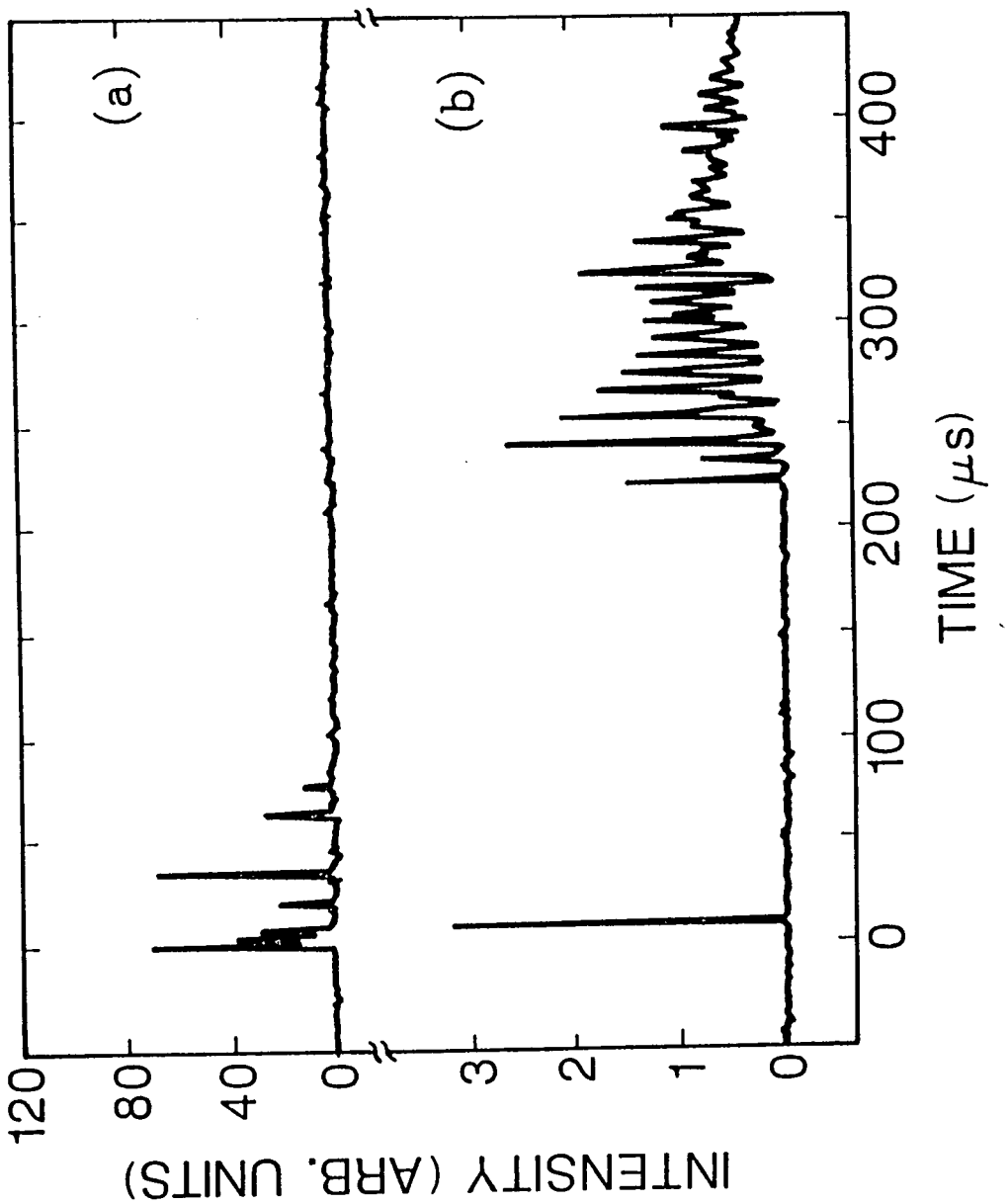
(a)
(b)
120
80
40
0
3
2
1
0
0
100
200
300
400
TIME (μs)
INTENSITY (ARB. UNITS)